

Coordination-dependence of hyperfine interactions at impurities on fcc metal surfaces.

II. Magnetic hyperfine field

V. Bellini,^{1,*} S. Cottenier,^{2,†} M. Çakmak,^{2,3} F. Manghi,¹ and M. Rots²¹*INFN-National Research Centre on nanoStructures and bioSystems at Surfaces (S3) and Dipartimento di Fisica, Università di Modena e Reggio Emilia, Via Campi 213/A, I-41100 Modena, Italy*²*Instituut voor Kern-en Stralingsfysica, Katholieke Universiteit Leuven, Celestijnenlaan 200 D, B-3001 Leuven, Belgium*³*Department of Physics, Gazi University, Teknikokullar, Tr-06500 Ankara, Turkey*

(Received 24 May 2004; published 29 October 2004)

We present a comparison between *ab initio* calculations and a high-quality experimental data set (1990–2002) of magnetic hyperfine fields of Cd at different sites on Ni surfaces. The experimentally observed parabolic coordination number dependence of this hyperfine field is verified as a general trend, but we demonstrate that individual cases can significantly deviate from it. It is shown that the hyperfine fields of other *5sp* impurities at Ni surfaces have their own, typical coordination number dependence. A microscopic explanation for the different dependencies is given in terms of the details of the *s*-DOS near the Fermi level.

DOI: 10.1103/PhysRevB.70.155419

PACS number(s): 68.47.De, 68.35.Fx, 68.35.Dv, 75.70.Rf

I. INTRODUCTION

The class of experimental techniques which uses nuclear probe atoms, such as Mössbauer spectroscopy, Perturbed Angular Correlation spectroscopy (PAC), and Nuclear Magnetic Resonance (NMR), plays an important role in the study of the electronic and magnetic properties of materials.^{1–6} What is most rewarding in these methods is their ability to probe simultaneously both charge symmetry related properties, such as the electric field gradients (EFG), as well as magnetic properties, such as magnetic hyperfine fields (HFF). While for the EFG commonly accepted guidelines for site identification on (100) and (111) metal surfaces were derived from experiments, and understood and extended by *ab initio* calculations,⁷ no universal trends exist for the HFF. Indeed, the HFF have been found to depend strongly on the type of probe atom (magnetic or nonmagnetic) as well as on the elements composing the magnetic host.⁸

In this respect, parameter-free *ab initio* band structure calculations have assumed a critical role in providing models to the experimental community, and assisting in the interpretation of the experimental results. For instance, the general behavior of the HFF induced on *sp*- and *d*-impurities embedded in bulk magnetic materials, especially in Fe and Ni, has been well characterized and the calculated values compared fairly well with the experimental ones.^{9–14} Selected calculations have been performed on more exotic systems. To name a few, the HFF on a Cd impurity atom at Fe/Co¹⁵ and Fe/Ag^{16,17} interfaces have been studied, focusing on the relation between the HFF induced on the radioactive probe atom and the magnetic moment profile across the interface. Similar studies have been performed on magnetic nanoclusters embedded in Ag¹⁸ and Cu¹⁹ matrices. In thin layers of *fcc* Fe on a Cu substrate, HFF and EFG at the surface and interface have been calculated.²⁰

If, for a few host materials, the dependence of HFF on the atomic number of the impurity atom has been studied in detail, less investigated is the variation in these properties for one specific probe atom in different environments derived

from the same host material. An example of such a study—motivated by the unique capability of nuclear probe techniques to follow the diffusion of single atoms—is provided by the experiments of Voigt *et al.*,⁵ recently extended and completed by Potzger *et al.*²¹ Those authors put a Cd atom at different low-index Ni-surfaces and at kinks and steps on those surfaces, and measured the HFF at the Cd probe atoms. Overlooking the now fairly complete data set, Potzger *et al.* conclude that the HFF at Cd depends more or less parabolically on the *number* of Ni-atoms in the first nearest neighbor shell (NN-shell) (black dots in Fig. 1), and not on the *exact position* of those Ni-neighbors (dubbed “symmetry independence of the HFF” in Ref. 22). This is attributed to a gradual change in the local DOS, not further specified. Our main goal in the present paper is to assess the validity of this claim, to elucidate the possible physical mechanism behind it (Sec. III A), and to try to extend this “rule” to impurity atoms other than Cd (Sec. II B), all this by calculating the HFF’s at Cd in different Ni-environments by *ab initio* methods. This is the second paper of a series of two. In the first

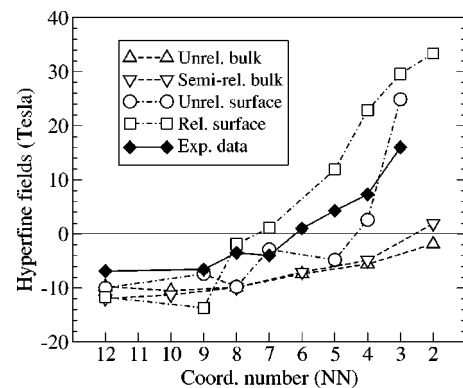


FIG. 1. Calculated coordination number (NN) dependence of the Cd hyperfine field in Ni hosts. Triangles (up and down) refer to simulations with bulk cells, while circles and squares are relative to the surface cells. Details of the cells are given in the text and in Table I.

paper of the series (Ref. 7) we have focused attention on the site identification—by means of EFG calculations—of Cd atoms on low-index fcc metal surfaces [(100), (110), and (111)], and demonstrate how commonly accepted experimental rules are in fact a manifestation of a simple coordination dependence mechanism. This mechanism was then subsequently generalized to other $5sp$ impurities. Our work follows pioneering cluster calculations by Lindgren *et al.*,^{23–26} who investigated HFF and EFG of Cd as an adatom or in a terrace site at (100) and (111) Ni surfaces, and a more systematic work by Mavropoulos *et al.*²⁷ on the HFF for probe atoms belonging to the whole $4sp$ series (Cu to Sr), placed on Ni and Fe (100) surfaces. Independent from our work, some of the questions that will be discussed here were studied very recently by Mavropoulos²⁸ using a different method (full-potential KKR), a different exchange-correlation functional (LDA), and not considering atomic relaxations.

II. METHOD AND DETAILS OF THE CALCULATIONS

We have employed a state of the art first-principles techniques, developed within the Density Functional Theory (DFT).^{29–31} Most of the calculations have been performed using the full-potential augmented plane wave+local orbitals (APW+lo) method^{31–33} as implemented in the WIEN2k package.³⁴ We have taken into account atomic relaxations since, as shown in the literature, they induce important effects in close-packed matrices to the HFF's.^{12,13} We have speed up such computationally expensive calculations by using a combination of methods. First, the atomic positions were relaxed using the pseudopotential plane wave VASP code.^{35,36} The all-electron APW+lo code was then used in a second stage to further relax the atoms to their equilibrium positions (with forces less than 1 mRy/a.u.), and to calculate the HFF. We have simulated sites with different coordination numbers using both bulk cells ($2 \times 2 \times 2$ periodicity = 32 atoms) and surface supercells with slabs with various thicknesses and in-plane periodicities. For a discussion on the convergence of the calculated quantities (EFG and HFF) with the size of the cells, as well as on the other details and parameters of the calculations, i.e., muffin tin radii, energy cut-off, Brillouin zone sampling, etc. ..., we refer the reader to Sec. II of the first paper of this series.⁷

Before proceeding with the discussion of the results, it is important to assess the accuracy of our calculated HFF's. To this end, let us look at an experimentally well-known case: Cd in bulk Ni, for which the experimental HFF at 4.2 K is -6.9 T.³⁷ To mimic as good as possible the situation of an isolated impurity in bulk Ni, we have considered two different supercells: a $2 \times 2 \times 2$ cell where the Cd impurities are arranged in a simple cubic sublattice (31 Ni and 1 Cd in the primitive cell, Cd–Cd distance of 7.02 Å), and a $4 \times 4 \times 4$ cell with Cd arranged in a face centered cubic sublattice (63 Ni and 1 Cd in the primitive cell, Cd–Cd distance of 9.93 Å). The Cd HFF's attain values of -9.8 T and -9.3 T, respectively, for the 32-atom and 64-atom supercells, when all Cd and Ni atoms are on ideal fcc positions. When we allow the Ni neighbors to move to new equilibrium positions as a reaction on the presence of the Cd-impurity, the

Cd-HFF's change to -12.0 T (32 atoms, first shell of Ni neighbors relaxed) and -11.7 T (64-atoms, 3 shells of Ni neighbors relaxed). The Cd–Cd distance in both our cells is large compared to the impurity-impurity distance used in previous supercell studies for different magnetic hosts, for which good agreement with experimental HFF's have been found: 5.71 Å for bcc-Fe^{13,14} and 6.10 Å for fcc-Co.¹⁴ In a recent paper by Haas,¹⁴ the Cd HFF's in a small (16 atoms) and in a very large (128 atoms) relaxed bulk Ni supercell were reported to be -12.3 and -9.2 T, respectively (in contrast to our calculations, the supercell lattice constant was allowed to vary in order to model better the long-range relaxation). These values are comparable to our results. We therefore conclude that most of the 5 T discrepancy with experiment does not have its origin in the artificial (small) interaction between the impurity atoms induced by the supercell technique, and we must attribute the difference with experiment mainly to the approximations contained in the chosen exchange-correlation functional, i.e., GGA. The 5 T error is similar to the 4.2 T overestimation of the HFF for Cd in Fe, and is of the same magnitude as was found for all 5th period impurities in Fe.^{12,13} As suggested by Haas,¹⁴ this is an absolute error that becomes particularly relevant, in proportion, in the case of a Ni host, where, due to a lower magnetization compared to Co and Fe, the impurities feel smaller HFF's.

Finally, for the 32-atom cell we have done also a calculation including SO-coupling (in contrast to all other calculations reported in this paper), from which we could obtain the orbital and dipolar contributions to the hyperfine field (the Ni-moment was put in the [111] direction, as in nature). They were smaller than 0.01 T, however, as could be expected for a closed shell atom as Cd ($[\text{Kr}]5s^24d^{10}$), such that the so-called Fermi contact term³⁸ is the only contribution to the HFF.

III. MAGNETIC HYPERFINE FIELDS

Two main questions will be addressed in the next sections. First, we want to verify and understand the experimentally proposed parabolic dependence of the Cd HFF on the number of Ni neighbors in the first coordination shell (NN), and we examine whether and how the spatial arrangement of these neighbors influences the HFF. As a second problem, we broaden the scope to the entire $5sp$ series, placing $5sp$ impurity atoms only in NN=4 (adatom) and NN=8 (terrace) coordinated sites at the Ni(100) surface. This will allow us to generalize the behavior observed for Cd to other probe atoms, and to propose qualitative explanations on the mechanisms ruling the observed HFF's.

A. Cd HFF's on Ni surfaces

In this section we focus on Cd probe atoms, placed in terrace and adatom positions at the three low-Miller-index surfaces of *fcc* Ni. This gives access to 6 differently coordinated sites, in addition to the fully coordinated substitutional bulk site and to a more artificial bridge site with NN=2. In order to test the sensibility of the HFF on the details of the

TABLE I. Hyperfine fields (T) of Cd in different Ni-environments. Experimental values are taken from Ref. 21. NN is the coordination number, and the “Type of cell” column supplies the cell dimensions, in units of the Ni lattice constant. The environment labeled as “bulk” refers to a single Cd impurity in a $2 \times 2 \times 2$ Ni supercell, while in the “bulk-like” environments a number of Ni nearest neighbors have been removed from the $2 \times 2 \times 2$ supercell. All other calculations (where Miller indices are given) have been carried out with slab supercells (see the text for details).

	#NN	Type of cell	Hyperfine fields (in T)		Exp
			Nonrelaxed	Relaxed	
Bulk	12	($2 \times 2 \times 2$)	-9.8	-12.0	-6.9
(100) Bulk		($2 \times 2, 7$ L)	-10.0	-11.7	
(111) Terrace	9	($\sqrt{2} \times \sqrt{2}, 7$ L)	-7.4 (12.18 Å)	-13.7 (10.49 Å)	-6.6
(100) Terrace	8	($2 \times 2, 5$ L)	-9.8(7.02 Å)	-1.9(5.80 Å)	-3.5
		($2 \times 2, 7$ L)	-8.3 (7.02 Å)	-6.7 (5.82 Å)	
		($\sqrt{2} \times \sqrt{2}, 7$ L)	-3.6(13.19 Å)	-5.9(11.88 Å)	
Bulk-like (“random”)		($2 \times 2 \times 2$)	-9.9	—	
Bulk-like (terrace)		($2 \times 2 \times 2$)	-8.2	—	
<i>bcc</i> -bulk		($2 \times 2 \times 2$)	-8.9	—	
(110) Terrace	7	($2 \times \sqrt{2}, 7$ L)	-2.9 (7.45 Å)	1.1 (5.66 Å)	4.1
		($2 \times 2\sqrt{2}, 9$ L)	-6.8(7.45 Å)	—	
(110) Adatom	5	($2 \times \sqrt{2}, 5$ L)	-4.8 (7.45 Å)	11.9 (6.91 Å)	4.3
		($2 \times \sqrt{2}, 7$ L)	-14.2(7.45 Å)	-6.5(6.93 Å)	
		($2 \times 2\sqrt{2}, 7$ L)	-21.7(7.45 Å)	—	
(100) Adatom	4	($2 \times 2, 5$ L)	-6.5(7.02 Å)	-3.6(6.51 Å)	7.3
		($2 \times 2, 7$ L)	3.4(7.02 Å)	38.7(6.63 Å)	
		($\sqrt{2} \times \sqrt{2}, 5$ L)	—	15.9(9.35 Å)	
		($\sqrt{2} \times \sqrt{2}, 7$ L)	2.6 (9.67 Å)	22.9 (9.28 Å)	
		($\sqrt{2} \times \sqrt{2}, 9$ L)	—	31.9(9.35 Å)	
		($\sqrt{2} \times \sqrt{2}, 11$ L)	—	25.1(9.35 Å)	
Bulk-like (“random”)		($2 \times 2 \times 2$)	-5.6	—	
Bulk-like (adatom)		($2 \times 2 \times 2$)	8.0	—	
Bulk-like (free layer)		($2 \times 2 \times 2$)	-4.2	—	
<i>bcc</i> Bulk-like (adatom)		($2 \times 2 \times 2$)	-9.6	—	
(111) Adatom	3	($2\sqrt{2} \times 2\sqrt{2}, 5$ L)	24.9 (8.11 Å)	31.9 (7.92 Å)	16.0
(111) Adatom	2	($\sqrt{2} \times \sqrt{2}, 7$ L)	n.p.	33.4 (8.26 Å)	—

cells, we performed also several calculations by varying the cell size and number of Ni layers in the slab. All the calculated Cd HFF for the differently coordinated systems are summarized in Table I and Fig. 1. Details on the cell are given in the format: (2D cell size, number of Ni layers). The Cd-Cd distance through the vacuum spacer is given in parentheses after the HFF values. The long hyphen “—” is used to label cases that were not calculated. The NN=2 coordinated site has been achieved by placing the Cd atom in a noncrystallographic adatom position on Ni(111). An “ideal unrelaxed position” has therefore no meaning for Cd on this site, which is indicated by the label “n.p.” (“not possible”). For the fully coordinated bulk site (NN=12), both a bulk and a slab calculation are reported, the latter with the Cd placed in the middle layer of the Ni slab. The experimental results of Potzger²¹ are reported in the last column. We first discuss the unrelaxed calculations, where all the atoms (including Cd) sit at their ideal *fcc* position. The calculated values predict for the Cd HFF a change in sign for mid-coordination and large

positive values for low coordination, in agreement with the experimental assignments. Changing the size of the slab, by adding Ni layers or by increasing the extension of the cells in the surface plane, results in some scattered values which lay, except for NN=5 and to a lesser extent also for NN=4, within the aforementioned expected precision (± 5 T). For the NN=5 case, i.e., adatom position at the Ni(110) surface, the HFF’s are found to attain large negative values for some of the considered cells. We will come back to these puzzling results later on.

As already discussed before, lattice relaxations are expected in such open systems and might induce important changes to the HFF’s. In fact it has been shown recently that their inclusion improves the agreement with the experimental data, in the case of *5sp* and *6sp* impurities in *bcc* bulk Fe.^{12,13} Due to the larger atomic volume of Cd with respect to Ni, an outward relaxation away from the surface is expected for both terrace and adatom positions, for all low-index surfaces. Our calculations show Cd displacements

TABLE II. Cd perpendicular relaxation (in Å) from an ideal *fcc* crystallographic site for the three low-index Ni surfaces. Everywhere Cd moves towards the vacuum.

Site	(100)	(110)	(111)
Adatom	0.20	0.26	0.09
Terrace	0.60	0.90	0.84

from ideal *fcc* positions towards the vacuum, that range from 0.60 to 0.90 Å for the terrace atom and from 0.09 to 0.26 Å for the adatom, depending on the surface orientation (Table II). Displacement for the terrace site are larger than for the adatom site: the Cd atom strives for a Cd—Ni bond length of about 2.65 Å (an observation taken from our 32-atom bulk calculation), that is somewhat larger than the ideal *fcc* Ni-Ni bond length of 2.48 Å. Starting from an adatom position, this can be realized with less displacement. Minor relaxations appear also in the Ni atoms around the impurity. As evident from Table I, the correction due to the relaxation is mostly within 7 T (except for NN=4 with corrections up to 35 T; see later). The correction is negative for the highest coordination numbers (NN=9 and 12) and positive for all others.

For a better comparison, the theoretical results for the unrelaxed and relaxed systems are plotted in Fig. 1 together with the experimental results. When more than one value exists in Table I, the ones relative to the cell with the largest volume are selected, except for the more sensitive NN=4 and NN=5 cases where the values closer to the experiments are chosen (this will be justified below). The chosen HFF's are given in bold in Table I. As evident from Fig. 1, upon relaxation of the atoms in the cell the barycenter of the HFF curve moves towards more positive values for NN>9, inducing a sign change already for NN=7 [Cd on a Ni(110) terrace site]. The largest changes are seen for NN=4 and NN=5, indicating once more a high sensitivity of these environments. No clear overall improvement is found when relaxations are included, and the experimental data lay somewhat between the relaxed and unrelaxed theoretical curves.

In order to investigate the reason for the large variations seen for the NN=4 and NN=5 coordinated sites, it is fruitful to look at the partial Density Of States (DOS) of Cd with *s*-symmetry (only *s*-electrons contribute to the HFF). In Fig. 2 the majority and minority *s*-DOS of a relaxed Cd adatom on Ni(100) is shown in a small energy window in the vicinity of the Fermi energy. The *s*-DOS shows several structures, among them a pronounced peak which for the majority channel lays right at E_F while it remains above E_F for the minority channel. Small variations in the details of the cell (number of layers, 2D cell size, relaxation or not, ...) or in the computational method (LDA/GGA, APW+lo or KKR, ...) will push this peak in the majority channel below or above E_F . Since only the majority spin is involved, one has a net change of the *s* spin magnetic moment, and – because this is roughly proportional to the HFF – also a change of the HFF itself. This is illustrated in Fig. 2 by an LDA-calculation for exactly the same cell as used for GGA. The majority *s*-peak for LDA is at a slightly higher energy than for GGA, leading

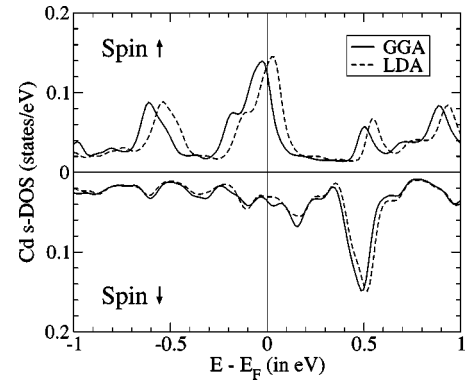


FIG. 2. Partial *s*-DOS for relaxed Cd on Ni(100) calculated in the LDA and GGA approximations.

to a reduced *s* spin moment of $1.05 \times 10^{-2} \mu_B$ ($2.02 \times 10^{-2} \mu_B$ for GGA). The corresponding HFF's are 20.4 T (LDA) and 38.7 T (GGA). As also in the LDA calculation this *s*-peak remains at E_F , it can be expected that using LDA throughout will not remove the sensitivity problem for NN=4 or 5, which is indeed what we observe. As a general rule, whenever such a peak is observed so close to E_F , an enhanced sensitivity of the HFF is foreseen, which adds to the inner precision of the calculations. For NN=4 and NN=5, we do observe such a peak in the *s*-DOS, for the other environments this is not the case. This explains the instability and wide scattering of the HFF's for those two coordination numbers in Table I (note that this instability does not affect the calculations for the EFG, which is ruled by *p*- rather than *s*-electrons). For impurity elements other than Cd, it might be that such sensitivity does not show up at all, or—if it does—it might do so for other values of the coordination number, depending on the details of the *s*-DOS close to E_F . The experimental values in Table I are up to 20 T below the calculated values for NN \geq 4. This indicates that in nature the majority *s*-peak is above E_F , while in our calculations it is below.

We now turn to the experimental parabolic NN-counting rule from Fig. 1. Both our relaxed and unrelaxed calculations show roughly the same trend (Fig. 1), and agree with the experimental trend. But how absolutely does this “parabolic rule” hold? Is it really true—as concluded by Potzger *et al.*²¹—that knowledge of the NN coordination is enough to predict the HFF on Cd in Ni-environments? In order to answer this question, we exploit the advantage of *ab initio* calculations that one is not restricted to environments that necessarily have to exist in nature. We can easily create artificial Cd-in-Ni-environments with an arbitrary number of nearest neighbors. That allows us to test the NN-counting rule in more situations than are experimentally accessible. The environments we created are $2 \times 2 \times 2$ supercells for Cd in bulk Ni, with a given amount of nearest neighbor Ni atoms removed (such that vacancies remain). This removal was done pair by pair, with the requirement that the remaining cell still has inversion symmetry (out of the several possibilities for every NN, we calculated only one). This requirement makes such environments essentially different from the corresponding surface environments with the same NN, because the

latter inevitably do not have inversion symmetry. In a first series, we start from the relaxed 32-atom Cd-in-Ni supercell as calculated before (labeled as “semi-relaxed,” because after removal of the Ni atoms no further relaxation is done), in a second series all atoms are at the ideal Ni bulk positions. The results of both series are almost identical, and are reported in Fig. 1. Clearly, the same trend as in experiment and as in the surface calculations is present in the artificial bulk calculations. This proves that there is a basic truth in the NN-counting rule. On the other hand, the large difference between the bulk and surface calculations—especially for the low-coordination environments—is a clear sign that contributions from higher coordination shells are not negligible.

If the requirement of inversion symmetry is removed, we can bridge the gap between these bulk-like cases and the surface slabs by calculating bulk-like cells where the first coordination shell is exactly the same as on a specific surface site. We did this for NN=8 and NN=4 (Table I, the environment labeled as “random” is the one with inversion symmetry). For NN=8, we could simulate in this way an environment that has exactly the same NN-coordination as the (100) terrace site. If the NN-counting rule was absolutely valid, we would find exactly the same HFF in the random and terrace-like bulk case. The results are indeed quite close: -9.9 T and -8.2 T, which are values that are also not far from the slab calculation (-8.3 T). An even more daring test of the counting rule is to put Cd at a substitutional site of an unrelaxed hypothetical *bcc* Ni $2 \times 2 \times 2$ supercell (16 atoms), with a lattice constant chosen such that the Ni-Ni distance (and hence also the unrelaxed Cd-Ni distance) is the same as in the *fcc* case. Even in this very different kind of environment, the calculated HFF of -8.9 T follows the simple counting rule. All this is different for NN=4. Apart from the random environment (-5.6 T), we tested a configuration that is identical to the *fcc* (100) adatom case (8.0 T), a configuration with all 4 Ni plus Cd in the same plane (a free layer, -4.2 T), and in a *bcc* cell a configuration that is identical to a *bcc* (100) adatom (-9.6 T). These 4 numbers prove that—even in *fcc*-based environments only—the exact spatial configuration of the Ni neighbors in the first coordination shell can be important, leading to differences of more than 13 T. It is not surprising to find this effect for NN=4 rather than NN=8, the former being identified before as a sensitive case. From this analysis we conclude that although the NN-counting rule certainly indicates a trend, there can be substantial deviations from it for specific environments. In such sensitive environments, the spatial arrangement of the neighbors is important as well. There is probably some luck involved that for Cd in Ni the behavior in nature is so smooth as experimentally observed, and there is no fundamental reason why the data could not have been considerably more scattered around the parabolic trend.

B. HFF's of the 5sp series

As a last part of this study we now present a survey for the 5sp impurities from Cd to Ba in Ni-environments, to see if and how the NN-counting rule can be extended to other impurities. We use the strategy applied by Mavropoulos *et al.*

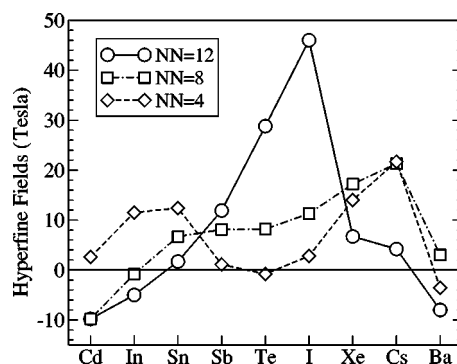


FIG. 3. Hyperfine fields of the entire 5sp series (Cd \rightarrow Ba) in bulk Ni (circle, NN=12), at a terrace position (squares, NN=8) and at an adatom position (diamonds, NN=4) on the Ni(100) surface.

*al.*²⁷ for 4sp impurities on Fe and Ni surfaces, and very recently and independently from this work also for 5sp impurities on Ni surfaces.²⁸ We take the bulk environment (NN=12) and the terrace (NN=8) and adatom (NN=4) environments for the (100) surface, and calculate the HFF for the 9 elements from Cd to Ba in those environments. The cell sizes chosen for those calculations are the ones labeled as in Table I as $(2 \times 2 \times 2)$, $(2 \times 2, 5 L)$, and $(2 \times 2, 7 L)$, respectively. Because we are looking for gross trends now and not for fine details, relaxations were not included. The results for the 5sp HFF's are displayed in Fig. 3. Exactly the same behavior as Mavropoulos *et al.* observed for 4sp and 5sp impurities is seen here, which mutually supports the validity of the very different computational methods that were used. In the bulk environment, the HFF starts at about -10 T for Cd, strongly increases with increasing atomic number Z , and reaches a maximum near the middle of the series: ≈ 46 T for *I*. Then it decreases again, and at the end of the series turns back to values close to -10 T. This behavior is in agreement with recent bulk calculations for relaxed 128-atom supercells (see Ref. 14, where also the comparison with experiment is discussed). When the coordination number is reduced, the main peak of the HFF curve moves to heavier elements and an additional structure—that for NN=8 is more a broad shoulder than a peak—appears at the beginning of the series. For NN=4 two clear structures are evident, and the HFF increases and decreases twice (with less intense variations than for the bulk) in the course of the 5sp series.

The microscopic origin of Fig. 3 can be understood by a slight extension of arguments given by Mavropoulos *et al.*²⁷ for 4sp impurities. Later on, we will derive from them (and test) generalized NN-counting rules for all 5sp impurities in Ni environments. For a systematic explanation, let us go back to the origin of hyperfine fields in ferromagnets (see Ref. 9 for a detailed and instructive review). As the hyperfine field in our cases is dominated by the Fermi contact contribution, we have to care about the details of the bond between the 5sp states and its environment (here Ni-3d). It has been known for a long time^{39,40} that in the case of such an *s-d* bond the local *s*-DOS of the impurity shows a characteristic depression a few eV below the Fermi energy: the “antiresonance dip” (AR). The position of the AR is mainly determined by the host material (Ni), and not by the impurity. The

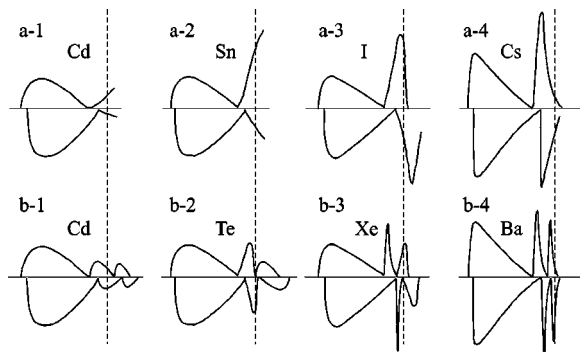


FIG. 4. Cartoons for the majority and minority partial s -DOS of (a) a $5sp$ impurity in bulk Ni and (b) a $5sp$ impurity at a Ni surface (low coordination, e.g., $NN=4$). The vertical line indicates the Fermi energy, the name of the elements indicates for which element a particular picture is representative. This picture is inspired by Ref. 9.

states below the AR are bonding states; the states above are antibonding. The up and down states are exchange split, such that at first sight one expects an excess of s -up over s -down, resulting in a positive hyperfine field. Due to a different s - d hybridization for up and down electrons, however, the number of s -up below AR will be diminished, while the number of s -down will be enhanced. Above AR, the situation is opposite.⁴¹ The final result is that the impurity s -moment (and hyperfine field) will be negative in the beginning of the sp -series, where the effect of the bonding states is dominant (Fig. 4-a-1). In the second half of the series, also the antibonding states will get filled, and because they have to be squeezed between AR and the Fermi energy, they have to develop a sharp peak in the DOS. The exchange splitting of this peak is responsible for the large positive HFF at the end of the sp -series (Fig. 4-a-2/3), which quickly drops to small and negative values again if also the down antibonding states are below the Fermi energy (Fig. 4-a-4). Mavropoulos *et al.* have shown by group theoretical arguments that in the case of reduced point group symmetry for the impurity (as on surfaces), the antibonding part of the impurity s -DOS is split in two parts. This splitting is more pronounced if the impurity is in more non-bulk-like environments, i.e., it is more pronounced for $NN=4$ than for $NN=8$. Let us take the $NN=4$ case with a clear splitting. When going from Cd to Ba, we evolve through the different stages of Fig. 4(b), which explains the double-peak structure of the HFF for $NN=4$ in Fig. 3.

An aspect of Fig. 3 that has not been discussed by Mavropoulos *et al.* is the physical origin of the coordination number dependence of the HFF for a particular element: why is, e.g., for In the $NN=4$ HFF the larger one and the $NN=12$ the smaller one, while this is reversed for, e.g., Te? This we will explain by the cartoon in Fig. 5. The upper part of Fig. 5 schematically shows the first of the two antibonding s -peaks of Fig. 4(b), for any particular impurity. If one lowers the coordination number of the impurity, the band-width of these peaks will decrease—an obvious fact, which we clearly observe in our calculations. Figure 5(a) shows the same situation for 3 typical band-widths: large ($NN=12$), medium ($NN=8$), and small ($NN=4$). The bottom part of

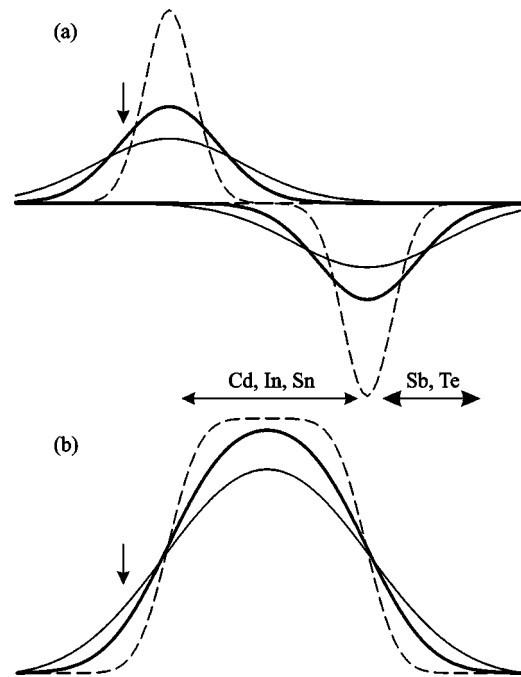


FIG. 5. (a) The first of the two antibonding s -peaks for majority and minority spin. (b) The s -moment derived from (a) by subtracting—at a particular energy—the integral of the minority s -DOS up to that energy from the integral of the majority s -DOS up to that energy. In both (a) and (b) 3 typical cases are drawn: high coordination = broad band width (thin full line), medium coordination = medium band width (thick full line) and low coordination = small band width (dashed line). The horizontal arrows indicate the region where the Fermi energy falls for the indicated elements (the first half of the $5sp$ -series). This story can be repeated with the second of the two antibonding peaks, starting from I for which the Fermi energy falls at the place indicated by the vertical arrow.

Fig. 5 shows the s spin moment derived from Fig. 5(a) as a function of energy (found by subtracting the integral of the down-peak from the integral of the up-peak, where the integrals are made up to the energy under consideration). Everything now depends on where the Fermi energy lies in Fig. 5. If it falls in the region indicated by Cd-In-Sn, Fig. 5(a) corresponds to Fig. 4-b-1. At the corresponding energy in Fig. 5(b), the s -moment (HFF) for the small band-width ($NN=4$) is larger than for the medium band-width ($NN=8$), which in turn is larger than for the large band-width ($NN=12$). If the Fermi energy falls in the region indicated by Sb-Te, Fig. 5(a) corresponds to Fig. 4-b-2 and the sequence of s -moments is reversed. After Te, this story repeats for the second antibonding peak (for I, the Fermi energy will be at the position marked by the vertical arrow, but of course in the second series of peaks), but will be increasingly less clear due to the presence of the $6s$ states that start to manifest themselves around the Fermi energy. That is the reason for the more chaotic evolution for Cs and Ba. Of course, Fig. 5 is a cartoon only, and its conclusions should not be taken too literally: the real DOS are not Gaussians as used in the cartoon, and therefore the details of the hyperfine field evolution might be different. Nevertheless, it captures the basic mechanism. Summarizing, we conclude that the physical mecha-

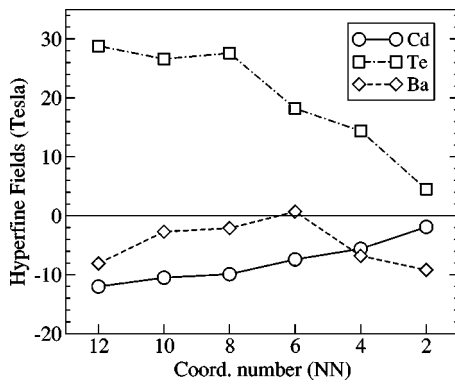


FIG. 6. Coordination dependence of the HFF for selected, i.e., Cd, Te and Ba, $5sp$ elements in Ni hosts, as obtained by bulk calculations (see the text for details).

nism behind Fig. 3 can be understood from a combination of three basic features: (i) the double peak structure of the antibonding peaks, (ii) the decrease in the band-width—and hence the increase of the peak height—upon reduction of the coordination number, and (iii) the position of the Fermi energy with respect to the peaks.

We now take Fig. 3 as a source of inspiration to extend the parabolic NN-counting rule proposed by Potzger *et al.* (Ref. 21) to $5sp$ impurities other than Cd. It can be seen from Fig. 3 that the Cd-HFF for bulk and NN=8 is almost the same and negative, while the value for NN=4 is small and positive: this is the parabolic behavior seen in experiment. In the same way, we can then deduce that for In and Sn as impurities, the HFF should monotonically rise from NN=12 to NN=4 (it is interesting to note that for the experimentally “easily” accessible Mössbauer probe ^{119}Sn , Fig. 3 suggests a linear behavior). Between Sn and Sb all lines cross, such that for Sb to I the HFF monotonically decreases from NN=12 to NN=4. For Xe to Ba, there is nonmonotonic behavior instead. We have checked this deduction by calculating the artificial bulk-like (nonrelaxed) environments as discussed before, but now for Te and Ba as impurities (both are taken as a representative for the region of monotonic decrease and the nonmonotonic region, just as Cd is a representative of the region of monotonic increase). In these bulk-like cells, we can more easily create environments with NN different from 4, 8, and 12. The results are given in Fig. 6. The general trends shown in Fig. 4 are the same as the ones which could

be inferred from the surface calculations of Fig. 3: a monotonic (parabolic) increase for Cd, a monotonic decrease for Te, and nonmonotonic behavior for Ba. In light of these results we therefore conclude that each of the $5sp$ impurities in Ni has its own typical coordination number counting rule.

IV. CONCLUSIONS

We have undertaken a comparison between *ab initio* calculations and a data set—experimentally collected during the past 15 years—of magnetic hyperfine fields of Cd at magnetic metallic fcc surfaces, i.e., Ni. The experimentally suggested parabolic-like coordination number dependence for the HFF of Cd at Ni surfaces is confirmed as being a reliable trend, but we warn that it is just a trend and not a rigorous rule: sensitive environments exist, for which the spatial arrangement of the Ni neighbors considerably influences the HFF. We have explained in detail the physical mechanism behind the HFF for all $5sp$ impurities at Ni surfaces, by combining knowledge from the literature and new insight. In particular we have generalized the parabolic NN-counting rule for Cd to other $5sp$ impurities, showing that each impurity has its own typical rule, and explaining why this is so. Together with the results on the EFG presented in the first paper of this series,⁷ we hope to have demonstrated that *ab initio* calculations can greatly enhance the physical insight in an experimentally complex problem.

ACKNOWLEDGMENTS

One of the authors (V.B.) acknowledges a fruitful discussion with Dr. K. Potzger. Part of the calculations were performed on computer facilities granted by an INFM project *Iniziativa Trasversale Calcolo Parallelo* at the CINECA supercomputing center. Another part of the computational work was performed on computers in Leuven, in the frame of projects G.0239.03 of the *Fonds voor Wetenschappelijk Onderzoek—Vlaanderen* (FWO), the Concerted Action of the KULeuven (GOA/2004/02) and the Inter-University Attraction Pole (IUAP P5/1). The authors are indebted to L. Verwilt and J. Knudts for their invaluable technical assistance concerning the pc-cluster in Leuven. M.C. thanks the *Onderzoeksfonds* of the KULeuven for financial support (F/02/010).

*Electronic address: Bellini.Valerio@unimore.it

†Electronic address: Stefaan.Cottenier@fys.kuleuven.ac.be

¹R. Vianden, in *Nuclear Physics Application on Materials Science*, edited by E. Recknagel and J. C. Soares (Kluwer Academic, New York, 1988), p. 239.

²G. Schatz, in Ref. 1, p. 297.

³G. Krausch, R. Fink, K. Jacobs, U. Kohl, J. Lohnmüller, B. Luckscheiter, R. Platzer, B.-U. Runge, U. Wöhrmann, and G. Schatz, *Hyperfine Interact.* **78**, 261 (1993).

⁴H. Haas, *Z. Naturforsch., A: Phys. Sci.* **50**, 407 (1994).

⁵J. Voigt, R. Fink, G. Krausch, B. Luckscheiter, R. Platzer, U. Wöhrmann, X. L. Ding, and G. Schatz, *Phys. Rev. Lett.* **64**, 2202 (1990).

⁶H. H. Bertschat, H.-H. Blaschek, H. Granzer, K. Potzger, S. Seeger, W.-D. Zeitz, H. Niehus, A. Burchard, D. Forkel-Wirth, and ISOLDE Collaboration, *Phys. Rev. Lett.* **80**, 2721 (1998).

⁷S. Cottenier, V. Bellini, M. Çakmak, F. Manghi, and M. Rots, *Phys. Rev. B* **70**, 155418 (2004).

⁸G. Rao, *Hyperfine Interact.* **24/26**, 1119 (1985).

⁹H. Akai, M. Akai, S. Blügel, R. Zeller, and P. H. Dederichs, J.

- Magn. J. Magn. Mater. **45**, 291 (1984).
- ¹⁰S. Blügel, H. Akai, R. Zeller, and P. H. Dederichs, Phys. Rev. B **35**, 3271 (1987).
- ¹¹H. Akai, M. Akai, S. Blügel, B. Drittler, H. Ebert, K. Terakura, R. Zeller, and P. H. Dederichs, Prog. Theor. Phys. Suppl. **101**, 11 (1990).
- ¹²T. Korhonen, A. Settels, N. Papanikolaou, R. Zeller, and P. H. Dederichs, Phys. Rev. B **62**, 452 (2000).
- ¹³S. Cottenier and H. Haas, Phys. Rev. B **62**, 461 (2000).
- ¹⁴H. Haas, Hyperfine Interact. **151/152**, 173 (2003).
- ¹⁵V. Bellini, R. Zeller, and P. H. Dederichs, Phys. Rev. B **64**, 144427 (2001).
- ¹⁶C. O. Rodriguez, M. V. Ganduglia-Pirovano, E. L. Peltzer y Blancá, M. Petersen, and P. Novák, Phys. Rev. B **63**, 184413 (2001).
- ¹⁷C. O. Rodriguez, M. V. Ganduglia-Pirovano, E. L. Peltzer y Blancá, and M. Petersen, Phys. Rev. B **64**, 144419 (2001).
- ¹⁸R. N. Nogueira and H. M. Petrilli, Phys. Rev. B **60**, 4120 (1999).
- ¹⁹S. Frota-Pessôa and S. Legoas, Hyperfine Interact. **133**, 207 (2001).
- ²⁰J. A. Gómez and D. Guenzenburger, J. Phys.: Condens. Matter **14**, 12311 (2002).
- ²¹K. Potzger, A. Weber, H. H. Bertschat, W.-D. Zeitz, and M. Dietrich, Phys. Rev. Lett. **88**, 247201 (2002).
- ²²M. J. Prandolini, Y. Manzhur, A. Weber, K. Potzger, H. H. Bertschat, H. Ueno, H. Miyoshi, and M. Dietrich, Appl. Phys. Lett. **85**, 76 (2004).
- ²³B. Lindgren, Hyperfine Interact. **34**, 217 (1987).
- ²⁴B. Lindgren, Europhys. Lett. **11**, 555 (1990).
- ²⁵B. Lindgren and A. Ghandour, Hyperfine Interact. **78**, 291 (1993).
- ²⁶B. Lindgren, Z. Naturforsch., A: Phys. Sci. **57**, 544 (2002).
- ²⁷Ph. Mavropoulos, N. Stefanou, B. Nonas, R. Zeller, and P. H. Dederichs, Phys. Rev. Lett. **81**, 1505 (1998).
- ²⁸Ph. Mavropoulos, J. Phys.: J. Phys.: Condens. Matter **15**, 8115 (2003).
- ²⁹P. Hohenberg and W. Kohn, Phys. Rev. **136**, 864 (1964).
- ³⁰W. Kohn and L. J. Sham, Phys. Rev. **140**, A1133 (1965).
- ³¹S. Cottenier, "Density Functional Theory and the Family of (L)APW-methods: A Step-By-Step Introduction," Instituut voor Kern- en Stralingsfysica, KULeuven, Belgium, 2002, ISBN 90-807215-1-4 (found at http://www.wien2k.at/reg_user/textbooks).
- ³²E. Sjöstedt, L. Nordström, and D. J. Singh, Solid State Commun. **114**, 15 (2000).
- ³³G. K. H. Madsen, P. Blaha, K. Schwarz, E. Sjöstedt, and L. Nordström, Phys. Rev. B **64**, 195134 (2001).
- ³⁴P. Blaha, K. Schwarz, G. Madsen, D. Kvasnicka, and J. Luitz, "WIEN2k, an augmented plane wave + local orbitals program for calculating crystal properties," Karlheinz Schwarz, Techn. Universität Wien, Austria, 1999, ISBN 3-9501031-1-2.
- ³⁵G. Kresse and J. Furthmüller, Comput. Mater. Sci. **6**, 15 (1996).
- ³⁶G. Kresse and J. Furthmüller, Phys. Rev. B **54**, 11 169 (1996).
- ³⁷D. A. Shirley, S. S. Rosenblum, and E. Matthias, Phys. Rev. **170**, 363 (1968).
- ³⁸E. Fermi, Z. Phys. **60**, 320 (1930).
- ³⁹K. Terakura, Prog. Theor. Phys. **46**, 1007 (1971).
- ⁴⁰K. Terakura, J. Phys. F: Met. Phys. **7**, 1773 (1977).
- ⁴¹E. Daniel and J. Friedel, J. Phys. Chem. Solids **24**, 1601 (1963).